AGU PUBLICATIONS

JGR

Journal of Geophysical Research: Space Physics

RESEARCH ARTICLE
10.1002/2016JA022411

Key Points:
- X-mode EM pump wave can excite PI near reflection height
- Parallel electric field is formed during X-mode EM wave propagating in ionosphere
- Numerical simulation for EM wave propagation in ionosphere modification experiment

Correspondence to:
C. Zhou,
chenzhou@whu.edu.cn

Citation:
Wang, X., P. Cannon, C. Zhou, F. Honary, B. Ni, and Z. Zhao (2016), A theoretical investigation on the parametric instability excited by X-mode polarized electromagnetic wave at Tromsø, *J. Geophys. Res. Space Physics, 121*, 3578–3591, doi:10.1002/2016JA022411.

Received 31 OCT 2015
Accepted 1 APR 2016
Accepted article online 7 APR 2016
Published online 18 APR 2016

A theoretical investigation on the parametric instability excited by X-mode polarized electromagnetic wave at Tromsø

Xiang Wang[1,2], Patrick Cannon[2], Chen Zhou[1], Farideh Honary[2], Binbin Ni[1], and Zhengyu Zhao[1]

[1]Department of Space Physics, School of Electronic Information, Wuhan University, Wuhan, China, [2]Department of Physics, Lancaster University, Lancaster, UK

Abstract Recent ionospheric modification experiments performed at Tromsø, Norway, have indicated that X-mode pump wave is capable of stimulating high-frequency enhanced plasma lines, which manifests the excitation of parametric instability. This paper investigates theoretically how the observation can be explained by the excitation of parametric instability driven by X-mode pump wave. The threshold of the parametric instability has been calculated for several recent experimental observations at Tromsø, illustrating that our derived equations for the excitation of parametric instability for X-mode heating can explain the experimental observations. According to our theoretical calculation, a minimum fraction of pump wave electric field needs to be directed along the geomagnetic field direction in order for the parametric instability threshold to be met. A full-wave finite difference time domain simulation has been performed to demonstrate that a small parallel component of pump wave electric field can be achieved during X-mode heating in the presence of inhomogeneous plasma.

1. Introduction

The ionospheric modification experiments, with high powerful high-frequency electromagnetic wave launched from the ground, have been performed since 1970s [*Utlaut and Cohen*, 1971; *Fialer*, 1974; *Minkoff et al*., 1974; *Thome and Blood*, 1974; *Robinson*, 1989; *Leyser and Wong*, 2009]. Both the ordinary and extraordinary polarized electromagnetic (EM) waves have been utilized to excite a range of plasma phenomena, such as high-frequency enhanced ion and plasma lines (HFILs and HFPLs) [*Frey*, 1986; *Rietveld et al*., 2000], artificial field-aligned irregularities (FAIs) [*Thome and Blood*, 1974; *Frolov et al*., 2014; *Blagoveshchenskaya et al*., 2011], enhanced airglow [*Bernhardt et al*., 1989; *Kosch et al*., 2002, 2007; *Pedersen and Carlson*, 2001; *Blagoveshchenskaya et al*., 2014], and stimulated electromagnetic emissions (SEEs) [*Stubbe et al*., 1984].

While the pump wave with ordinary polarization (O-mode) has been extensively studied to explain the excitation of parametric instability in the past decades [*Perkins et al*., 1974; *Fejer*, 1979; *Fejer and Leer*, 1972; *Kuo*, 1996, 2002, 2015; *Kuo et al*., 1983, 2014; *Bryers et al*., 2013], the extraordinary polarized (X-mode) pump wave has been considered not to be able to excite Langmuir wave near its reflection height due to the frequency matching condition not being satisfied [*Kuo*, 2015]. The issue with the excitation of Langmuir parametric decay instability (PDI) and Langmuir oscillating two-stream instability (OTSI) by X-mode heating is due to the fact that the plasma frequency near X-mode pump wave reflection height is less than the heater frequency, thus not satisfying the frequency matching condition. In addition, it has been known that the X-mode pump wave cannot parametrically excite the Langmuir wave propagating along the geomagnetic field because of the lack of parallel electric field component. However, recent experimental observations performed by the European Incoherent Scatter (EISCAT) heating facility at Tromsø, Norway, demonstrate that an X-mode pump wave can produce HF-enhanced plasma lines (HFPLs) and HF-enhanced ion lines (HFILs) [*Blagoveshchenskaya et al*., 2014, 2015], which indicate the excitation of parametric instability near the X-mode reflection height. The comparison between the temporal behaviors of HFPLs excited by O/X-mode pump wave indicates that for the case of X-mode heating, the HFPLs are observed throughout the whole heating cycle, in contrast to a short duration (on the order of few milliseconds) just after the heater is turned on under O-mode heating, as reported by *Blagoveshchenskaya et al*. [2014] (i.e., Figure 3, top plot). *Blagoveshchenskaya et al*. [2014] employed the reflection heights of ordinary/extraordinary-polarized EM pump waves to distinguish the HFPLs and HFILs excited by O-mode or X-mode pumping. As seen in Figure 4 by *Blagoveshchenskaya et al*. [2014], from 17:00 to 17:31 UT on 19 October 2012, the reflection heights of O/X-mode pump waves are close to 260 km and 250 km, respectively. Thus, the enhanced HFILs

and HFPLs observed during 17:16–17:26 UT ascribe to X-mode heating wave. *Blagoveshchenskaya et al.* [2015] report temporal behavior of HFPLs under the condition of $f_0/f_oF_2 = 0.91–1.31$, where f_0 is the X-mode pump wave frequency and f_oF_2 is the critical frequency of O-mode wave at F_2 layer. According to *Blagoveshchenskaya et al.* [2015], HFPLs are observed in the whole heating cycle under the X-mode frequency when the pump frequency is less than the critical frequency of X-mode wave in F_2, f_xF_2, whereas HFPLs are absent when the frequency of X-mode pumping f_0 exceeds f_xF_2. It is known that the HFPLs are related to the excited Langmuir wave propagating along the radar beam, while the zero-frequency offset HFILs symbolize the excitation of the OTSI. For example, *Muldrew and Showen* [1977] indicate that the Langmuir waves responsible for the HFPLs are excited at the height in the ionosphere where the HF electric field is at its maximum, i.e., at the main Airy maximum, just several hundred meters below the reflection height. *Senior et al.* [2013] suggest that only the higher-frequency X-mode pump wave can simultaneously excite HFILs and HFPLs.

In this paper, the plasma continuity equation, equation of motion, and Poisson's equation are employed to derive the excitation and the threshold of the Langmuir OTSI and PDI for X-mode pump wave. The derived equations have been used to calculate the parametric instability threshold for several recent experimental observations. In section 2, the four-wave interaction process for OTSI and the three-wave interaction process for PDI are analyzed. The possible excited plasma wave modes by X-mode pump wave are deduced, and the threshold expression is obtained. Section 3 compares the observations of the three experiments ran at EISCAT with the theoretical calculations. The threshold expressions deduced in section 2 require a minimum fraction of pump wave power to be directed along the geomagnetic field direction; in section 4, full-wave numerical simulations are used to test if these criteria could be met for the experimental conditions analyzed in section 3. The summary and conclusion are presented in section 5.

2. Parametric Instability Excited by X-Mode Pump Wave

2.1. Basic Theory

When a high powerful HF electromagnetic wave $\vec{E}_p\left(\Omega_0,\ \vec{k}_0\right)$ is injected into the ionospheric plasma, it acts as a pump wave to excite high- and low-frequency plasma waves simultaneously via the parametric coupling process. In parametric decay instability, the pump wave decays to a high-frequency plasma wave $\left(\Omega,\ \vec{k}\right)$ and a low-frequency plasma wave $\left(\Delta\Omega, \Delta\vec{k}\right)$. In the oscillating two-stream instability, the HF pump wave decays to two oppositely propagating high-frequency plasma waves $\left(\Omega_{\pm}, \pm\vec{k}\right)$ together with a purely growing mode $\left(\Delta\Omega, \Delta\vec{k}\right)$. The frequencies and wave vectors of the excited plasma waves are governed by the matching conditions:

$$\Omega_0 = \Omega_+ + \Delta\Omega^* = \Omega_- - \Delta\Omega \tag{1}$$

$$\vec{k}_0 = \vec{k} + \Delta\vec{k} = -\vec{k} - \Delta\vec{k} \tag{2}$$

where $\omega_{\pm}$ and $\pm\vec{k}$ are the wave frequencies and wave vectors of the high-frequency plasma waves, whereas $\Delta\omega$ and $\Delta\vec{k}$ represent the frequency and wave vector of the low-frequency electrostatic wave.

For the derivation of the threshold value for the excitation of parametric instability, the continuity equation, equation of motion, and Poisson's equation are employed in a set of coupled equations [*Baumjohann and Treumann*, 1996; *Gurevich*, 1978].

$$\frac{\partial}{\partial t} n_{e,i} + \nabla\cdot\left(n_{e,i}\vec{v}_{e,i}\right) = 0 \tag{3}$$

$$\left(\frac{\partial}{\partial t} + \upsilon_e\right)\left(n_e\vec{v}_e\right) + \Omega_e n_e\vec{v}_e\times\hat{z} = -\nabla\cdot\left(n_e\vec{v}_e\vec{v}_e\right) - \frac{e}{m_e}n_e\left(\vec{E}_p - \nabla\Phi\right) - \gamma_e v_{Te}^2\nabla\delta n_e \tag{4a}$$

$$\left(\frac{\partial}{\partial t} + \upsilon_i\right)\left(n_i\vec{v}_i\right) - \Omega_i n_i\vec{v}_i\times\hat{z} = -\nabla\cdot\left(n_i\vec{v}_i\vec{v}_i\right) + \frac{e}{m_i}n_i\left(\vec{E}_p - \nabla\Phi\right) - \gamma_i v_{Ti}^2\nabla\delta n_i \tag{4b}$$

$$\nabla^2\Phi = -\sum e_\alpha n_\alpha/\varepsilon_0 \tag{5}$$

where the subscripts e and i indicate the electron and ion; m, e, and T are the mass, charge, and temperature of the charge particles, respectively; δn is the disturbed density of particles; $n = n_0 + n_{\pm k} + n_{\pm \Delta k}$ is the total particle density, where n_0 is the undisturbed particle density and $n_{\pm k}$ and $n_{\pm \Delta k}$ are the disturbed particle densities associated with the excited high- and low-frequency plasma waves; $\vec{v} = \vec{v}_{k_0} + \vec{v}_{\pm k} + \vec{v}_{\pm \Delta k}$ is the particle velocity, where $\vec{v}_{k_0}, \vec{v}_{\pm k}$, and $\vec{v}_{\pm \Delta k}$ are the particle velocities driven by the pump wavefield, high-frequency plasma wavefield, and the low-frequency plasma wavefield respectively; $\vec{E}_p$ is the electric field of the pump wave; Φ is the electric potential of the excited electrostatic wave; $\Omega_{e,i} = e_{e,i}B_0/m_{e,i}$ are the charged particles (electron and ion) gyrofrequencies; $\vec{B}_0 = B_0\hat{z}$ is the undisturbed magnetic field strength, where the $\hat{z}$ axis is along the magnetic field direction; $v_{Te,Ti} = \sqrt{k_b T_{e,i}/m_{e,i}}$ is the thermal velocity of charge particle; $\gamma_{e,i}$ are the adiabatic indices for electron and ion, respectively; ε_0 is the free space permittivity and k_b is the Boltzmann constant; $\upsilon_e = \upsilon_{ei} + \upsilon_{en} + \upsilon_{eL}$ and $\upsilon_i = \upsilon_{ie} + \upsilon_{in} + \upsilon_{iL}$ are the electron and ion effective collision frequencies, respectively, where υ_{ei}, υ_{en}, υ_{ie}, and υ_{in} are electron-ion, electron-neutral, ion-electron, and ion-neutral collision frequencies, respectively; and electron and ion Landau damping are represented as [*Baumjohann and Treumann*, 1996]

$$\upsilon_{eL} = \Omega\sqrt{\pi/8}\,\Lambda_0^{3/2}(\eta_e)\exp\left[-1.5 - \Lambda_0(\eta_e)/2k_z^2\lambda_D^2\right]/\left(k_z^3\lambda_D^3\right)$$
$$\upsilon_{iL} = \Delta\Omega\sqrt{\pi/8}\left[(m_e/m_i)^{1/2} + (T_e/T_i)^{3/2}\exp(-T_e/2T_i - 3/2)\right]$$

where $\Lambda_0(\eta_e) = I_0(\eta_e)\exp(-\eta_e)$, $\eta_e = k_\perp^2 v_{Te}^2/2\Omega_e^2$, I_0 is the modified Bessel function, $\lambda_D = (\varepsilon_0 k_b T_e/n_0 e^2)^{1/2}$ is the electron Debye length, and k_z and $k_\perp$ are the parallel and perpendicular components of the wave vector $\vec{k}$ with respect to geomagnetic field, respectively. Although we analyze the excitation process from the fluid equations, the Landau damping term included in the effective collision frequency represents the kinetic effect.

The pump wavefield is assumed as $\vec{E}_p = \vec{E}_{k_0}\exp\left[i\left(\vec{k}_0 \cdot \vec{r} - \Omega_0 t\right)\right]/2$. Every physical quantity is treated as the sum of frequency components; e.g., $\vec{v} = \vec{v}_{(k_0,\Omega_0)} + \vec{v}_{(\pm k,\pm\Omega)} + \vec{v}_{(\pm\Delta k,\pm\Delta\Omega)}$, where the subscript is the exponent, likewise, $\vec{v}_{(\pm k,\pm\Omega)} = \vec{v}_k\exp\left[i\left(\vec{k}\cdot\vec{r} - \Omega t\right)\right] + \vec{v}_{-k}\exp\left[-i\left(\vec{k}\cdot\vec{r} - \Omega t\right)\right]$. Then, the physical quantities described by frequency components are incorporated into the original equations, and the terms of the same exponent are combined. The arbitrariness of $\vec{r}$ and t demands that the coefficient of each exponent term equals to zero. Thus, a series of equations of frequency components can be obtained to determine the dispersion relation equation of the parametric coupling process.

Concerning the $\left(\Omega_0, \vec{k}_0\right)$ wave mode, only electron can respond effectively to the pump wavefield, and then the component of the potential of plasma wave $\Phi_{k_0} = 0$, i.e., $\delta n_{k_0} = 0$; since the second term $(\vec{v}_k \cdot \nabla\vec{v}_{\Delta k})$ in the left hand of Eq. (4a) is very small, it can be neglected. Hence, the motion equation (4a) can be simplified to obtain the following equation:

$$\left(\frac{\partial}{\partial t} + \upsilon_e\right)\vec{v}_{k_0} + \Omega_e\vec{v}_{k_0} \times \hat{z} = -\frac{e}{m_e}\vec{E}_p \tag{6}$$

With the aid of the perpendicular component of equation (6), and taking the cross product of the equation (6) with $\hat{z}$, we obtain

$$\left(\frac{\partial}{\partial t} + \upsilon_e\right)\left[\left(\frac{\partial}{\partial t} + \upsilon_e\right)^2 + \Omega_e^2\right]\vec{v}_{k_0} = -\frac{e}{m_e}\left[\left(\frac{\partial}{\partial t} + \upsilon_e\right)^2\vec{E}_p + \Omega_e^2\vec{E}_{pz} - \left(\frac{\partial}{\partial t} + \upsilon_e\right)\Omega_e\vec{E}_p \times \hat{z}\right] \tag{7}$$

In $k - \omega$ domain, the above expression can be written as

$$\vec{v}_{k_0} = +i\,\frac{e}{m_e}\,\frac{(\Omega_0 + i\upsilon_e)^2\vec{E}_p - \Omega_e^2\vec{E}_{pz} - i(\Omega_0 + i\upsilon_e)\Omega_e\vec{E}_p \times \hat{z}}{(\Omega_0 + i\upsilon_e)\left[(\Omega_0 + i\upsilon_e)^2 - \Omega_e^2\right]} \tag{8}$$

When considering that only electrons respond to the high-frequency plasma wave, the set of equations (3)–(5) can be rewritten as

$$\frac{\partial}{\partial t}n_k + \nabla\cdot\left(n_0\vec{v}_k + n_{\Delta k}\vec{v}_{k_0}\right) = 0 \tag{9a}$$

$$\left(\frac{\partial}{\partial t}+\upsilon_e\right)n_0\vec{v}_k + \Omega_e n_0\vec{v}_k\times\hat{z} = -\left(3v_{Te}^2\nabla n_k - \frac{en_0}{m_e}\nabla\Phi_k\right) - \frac{en_{\Delta k}}{m_e}\vec{E}_p - \nabla\cdot\left(n_k\vec{v}_{k_0}\vec{v}_{k_0}^{\,*} + 2n_0\vec{v}_{k_0}\vec{v}_k^{\,*}\right) - \left[\left(\frac{\partial}{\partial t}+\upsilon_e\right)n_{\Delta k}\vec{v}_{k_0} + \Omega_e n_{\Delta k}\vec{v}_{k_0}\times\hat{z}\right] \tag{9b}$$

$$\nabla^2\Phi_k = en_k/\varepsilon_0 \tag{9c}$$

With the aid of the equations (9a) and (9c), the orthogonal components of equation (9b) are combined into a scalar equation

$$\left[\left(\frac{\partial}{\partial t}+\upsilon_e\right)^2+\Omega_e^2\right]\left[\frac{\partial}{\partial t}\left(\frac{\partial}{\partial t}+\upsilon_e\right) - 3v_{Te}^2\nabla^2 + \Omega_{pe}^2 + \Omega_e^2\sin^2\theta\right]n_k$$

$$= + \left\{\left[\left(\frac{\partial}{\partial t}+\upsilon_e\right)^2\nabla + \Omega_e^2\nabla_z\right]\cdot\left\langle\vec{v}_{k_0}\cdot\nabla\vec{v}_{k_0}\right\rangle - \Omega_e\left(\frac{\partial}{\partial t}+\upsilon_e\right)\nabla\cdot\left\langle\vec{v}_{k_0}\cdot\nabla\vec{v}_{k_0}\right\rangle\times\hat{z}\right\}n_k$$

$$+\frac{e}{m_e}\left\{\left[\left(\frac{\partial}{\partial t}+\upsilon_e\right)^2\nabla + \Omega_e^2\nabla_z\right]\cdot\vec{E}_p - \Omega_e\left(\frac{\partial}{\partial t}+\upsilon_e\right)\nabla\cdot\vec{E}_p\times\hat{z}\right\}n_{\Delta k} \tag{10}$$

where $\Omega_{pe}^2 = e^2n_0/\varepsilon_0 m_e$ is the electron plasma frequency, θ is the angle between the wave vector $\vec{k}$ and the magnetic field $\vec{B}_0$, and $\langle\rangle$ stands for an average over the fast oscillation.

For the low-frequency decay mode, both electron and ion response are included to derive the dispersion relation. It is assumed that $n_{\Delta k}^e \approx n_{\Delta k}^i = n_{\Delta k}$ to satisfy quasi-neutrality in the low-frequency plasma field. The set of fluid equations for the low-frequency component $\left(\Delta\Omega, \Delta\vec{k}\right)$ for electron and ion are

$$\frac{\partial}{\partial t}n_{\Delta k} + \nabla\cdot\left(n_0\vec{v}_{\Delta k}^{\,e} + n_k\vec{v}_{k_0}\right) = 0 \tag{11a}$$

$$\left(\frac{\partial}{\partial t}+\upsilon_e\right)\left(n_0\vec{v}_{\Delta k}^{\,e}\right) + \Omega_e n_0\vec{v}_{\Delta k}^{\,e}\times\hat{z} = -\left(v_{Te}^2\nabla n_{\Delta k} - \frac{en_0}{m_e}\nabla\Phi_{\Delta k}\right) - \frac{e}{m_e}n_k\vec{E}_p - n_{\Delta k}\vec{v}_{k_0}\cdot\nabla\vec{v}_{k_0} - 2n_0\vec{v}_{k_0}\cdot\nabla\vec{v}_k - \left(\frac{\partial}{\partial t}+\upsilon_e\right)n_k\vec{v}_{k_0} - \Omega_e n_k\vec{v}_{k_0}\times\hat{z} \tag{11b}$$

$$\frac{\partial}{\partial t}n_{\Delta k} + \nabla\cdot\left(n_0\vec{v}_{\Delta k}\,i\right) = 0 \tag{11c}$$

$$\left(\frac{\partial}{\partial t}+\upsilon_i\right)n_0\vec{v}_{\Delta k}\,i - \Omega_i n_0\vec{v}_{\Delta k}\,i\times\hat{z} = -\left(3v_{Ti}^2\nabla n_{\Delta k} + \frac{en_0}{m_i}\nabla\Phi_{\Delta k}\right) \tag{11d}$$

The electron and ion fluid equations are combined respectively; i.e., equation (11a) combines with equation (11b) and equation (11c) combines with equation (11d). Thus,

$$\left[\left(\frac{\partial}{\partial t}+\upsilon_{es}\right)^2+\Omega_e^2\right]\nabla\cdot n_0\vec{v}_{\Delta k}\,e\times\hat{z} = -\Omega_e\left(v_{Te}^2\nabla_\perp^2 n_{\Delta k} - \frac{en_0}{m_e}\nabla_\perp^2\Phi_{\Delta k}\right)$$
$$-\Omega_e\frac{e}{m_e}\nabla_\perp\cdot n_k\vec{E}_p - \frac{e}{m_e}\left(\frac{\partial}{\partial t}+\upsilon_{es}\right)\nabla\cdot n_k\vec{E}_p\times\hat{z}$$
$$-\Omega_e\nabla_\perp\cdot\left(n_{\Delta k}\vec{v}_{k_0}\cdot\nabla\vec{v}_{k_0}\right) - \left(\frac{\partial}{\partial t}+\upsilon_{es}\right)\nabla\cdot\left(n_{\Delta k}\vec{v}_{k_0}\cdot\nabla\vec{v}_{k_0}\right)\times\hat{z}$$
$$-\Omega_e\nabla_\perp\cdot\left(2n_0\vec{v}_{k_0}\cdot\nabla\vec{v}_k\right) - \left(\frac{\partial}{\partial t}+\upsilon_{es}\right)\nabla\cdot\left(2n_0\vec{v}_{k_0}\cdot\nabla\vec{v}_k\right)\times\hat{z} - \left(\frac{\partial}{\partial t}+\upsilon_{es}\right)^2\nabla\cdot n_k\vec{V}_{k_0}\times\hat{z} - \Omega_e^2\nabla\cdot n_k\vec{V}_{k_0}\times\hat{z} \tag{12a}$$

$$\left[\left(\frac{\partial}{\partial t}+\upsilon_{is}\right)^2+\Omega_i^2\right]n_0\nabla\cdot\underset{\Delta k}{\vec{v}}\,i\times\hat{z}=+\Omega_i\left(3v_{Ti}^2\nabla_\perp^2 n_{\Delta k}+\frac{en_0}{m_i}\nabla_\perp^2\Phi_{\Delta k}\right) \tag{12b}$$

Combining equations (11b) and (11d) and taking the expression from equation (12a), a set of coupled equations for the low-frequency decay mode can be written as:

$$\begin{aligned}&\left(\frac{\partial}{\partial t}+\upsilon_i\right)^2\left\{-\left[\left(\frac{\partial}{\partial t}+\upsilon_e\right)^2\nabla^2+\Omega_e^2\nabla_z^2\right]\left[\frac{\partial}{\partial t}\left(\frac{\partial}{\partial t}+\upsilon_i\right)-c_s^2\nabla^2\right]-\Omega_e\Omega_i\frac{\partial}{\partial t}\left(\frac{\partial}{\partial t}+\upsilon_e\right)\nabla_\perp^2\right\}n_{\Delta k}=\\&-\frac{m_e}{m_i}\left(\frac{\partial}{\partial t}+\upsilon_i\right)^2\nabla^2\left\{\left[\left(\frac{\partial}{\partial t}+\upsilon_e\right)^2\nabla+\Omega_e^2\nabla_z\right]\cdot\left\langle\underset{k_0}{\vec{v}}\cdot\nabla\underset{k_0}{\vec{v}}\right\rangle-\Omega_e\left(\frac{\partial}{\partial t}+\upsilon_e\right)\nabla\cdot\left\langle\underset{k_0}{\vec{v}}\cdot\nabla\underset{k_0}{\vec{v}}\right\rangle\times\hat{z}\right\}n_{\Delta k}\\&+\frac{m_e}{m_i}\left(\frac{\partial}{\partial t}+\upsilon_i\right)^2\nabla^2\left\{\begin{array}{l}-\frac{en_k}{m_e}\left[\left(\frac{\partial}{\partial t}+\upsilon_e\right)^2\nabla+\Omega_e^2\nabla_z\right]\cdot\underset{p}{\vec{E}}+\frac{en_k}{m_e}\Omega_e\left(\frac{\partial}{\partial t}+\upsilon_e\right)\nabla\cdot\underset{p}{\vec{E}}\times\hat{z}\\-\left[\left(\frac{\partial}{\partial t}+\upsilon_{es}\right)^2\nabla+\Omega_e^2\nabla_z\right]\cdot n_0\left\langle\underset{k_0}{\vec{v}}\cdot\nabla\underset{k}{\vec{v}}\right\rangle+\Omega_e\left(\frac{\partial}{\partial t}+\upsilon_e\right)\nabla\cdot n_0\left\langle\underset{k_0}{\vec{v}}\cdot\nabla\underset{k}{\vec{v}}\right\rangle\times\hat{z}\end{array}\right\}\end{aligned} \tag{13}$$

where $c_s=\sqrt{k_b(T_e+3T_i)/m_i}$ is the ion acoustic speed. From the electron motion equation (9b), the linear part of electron velocity $\underset{k}{\vec{v}}$ driven by the excited high-frequency wave is expressed in $k-\omega$ domain as

$$\underset{\pm k}{\vec{v}}=\pm\frac{e\Omega_{pe}^2}{m_e k^2}\frac{(\Omega+i\upsilon_e)^2\,\vec{k}-\Omega_e^2\underset{z}{\vec{k}}-i\Omega_e(\Omega+i\upsilon_e)\,\vec{k}\times\hat{z}}{(\Omega+i\upsilon_e)\left[(\Omega+i\upsilon_e)^2-\Omega_e^2\right]}\frac{n_{\pm k}}{n_0} \tag{14}$$

The left-hand sides of equations (10) and (13) define the dispersion relations of the excited high-frequency and low-frequency plasma waves, respectively, while the right-hand sides of equations (10) and (13) are the coupling terms driving the plasma waves.

The possible plasma mode excited by the X-mode pump wave in the parametric instability is deduced from the left-hand sides of equations (10) and (13) when the damping rate is neglected and the pump wavefield is absent. Furthermore, when the excited electrostatic waves propagate either parallel or obliquely with the magnetic field, i.e., $0\le\theta<\pi/2$, the left-hand sides of equations (10) and (13) reduce to

$$\Omega^2-3k^2v_{Te}^2-\Omega_{pe}^2-\Omega_e^2\sin^2\theta=0 \tag{15a}$$

$$\Delta\Omega^2\left(\Delta\Omega^2-k^2c_s^2\right)=0 \tag{15b}$$

Thus, the high-frequency sideband excited by parametric instability is Langmuir wave with a linear dispersion relation given by

$$\Omega^2=\Omega_L^2=\Omega_{pe}^2+\Omega_e^2\sin^2\theta+3k^2v_{Te}^2 \tag{16}$$

while the low-decay mode concurrently excited is the ion acoustic wave ($\Delta\omega=kc_s$) or the purely growing mode ($\Delta\omega=0$).

2.2. The Threshold of the Parametric Instability Near X-Mode Reflection Height

Decay of an X-mode EM wave $\underset{p}{\vec{E}}\left(\underset{0}{\vec{k}}\approx 0,\ \Omega_0\right)$ to a Langmuir wave and a purely growing or ion acoustic decay mode below the reflection height, where $\Omega_{pe}^2=\Omega_0(\Omega_0-\Omega_e)$, are studied as follows: the frequency and wave vector of Langmuir sideband are $\omega_\pm=\omega$ and $\underset{+}{\vec{k}}=-\underset{-}{\vec{k}}=\vec{k}$, where $\vec{k}=k_z\hat{z}+k_\perp\hat{x}$; the frequency and the wave vector of the high-frequency plasma wave are driven from the matching condition, i.e., $\omega=\omega_0-\Delta\omega$ and $\vec{k}=-\Delta\,\vec{k}$. In the interaction region, the X-mode EM wavefield is given by

$$\underset{p}{\vec{E}}=E_{z0}\hat{z}\exp(-i\Omega_0 t)+E_{\perp 0}(\hat{x}-i\hat{y})\exp(-i\Omega_0 t) \tag{17}$$

With the aid of equations (17), (10), and (13) in the $k-\omega$ domain become

$$\left[\Omega(\Omega+i\upsilon_e)-\left(3v_{Te}^2k^2+\Omega_{pe}^2+\Omega_e^2\sin^2\theta\right)\right]n_{\pm k}=$$
$$-\frac{e^2}{m_e^2\Omega_0^2}\frac{1-\Omega_e^2/\Omega_0^2}{1-\Omega_e^2\cos^2\theta/\Omega_0^2}\left\{\left(\vec{k}\cdot\vec{E}_{pz}\right)^2+\frac{1}{(1+\Omega_e/\Omega_0)(1-\Omega_e^2/\Omega_0^2)}\left(\vec{k}\cdot\vec{E}_{p\perp}\right)^2\right\}n_{\pm k}$$
$$\mp i\frac{e}{m_e}\frac{1-\Omega_e^2/\Omega_0^2}{1-\Omega_e^2\cos^2\theta/\Omega_0^2}\left\{\left(\vec{k}\cdot\vec{E}_{pz}\right)+\frac{1}{1+\Omega_e/\Omega_0}\left(\vec{k}\cdot\vec{E}_{p\perp}\right)\right\}n_{\pm\Delta k} \tag{18}$$

$$\left\{\begin{array}{l}+\Omega_e^2\left[\Delta\Omega(\Delta\Omega+i\upsilon_i)-k^2c_s^2\right](-k_z^2)\\ -\left\{\begin{array}{l}+(\Delta\Omega+i\upsilon_e)^2\left[\Delta\Omega(\Delta\Omega+i\upsilon_i)-k^2c_s^2\right]\\ -\Omega_e\Omega_i\Delta\Omega(\Delta\Omega+i\upsilon_e)\end{array}\right\}(-k_\perp^2)\end{array}\right\}n_{\Delta k}=$$
$$+\frac{m_e}{m_i}\frac{e^2\Omega_e^2}{m_e^2\Omega_0^2}k^2\left\{+\left(\vec{k}\cdot\vec{E}_{pz}\right)^2+\frac{\Delta\Omega}{\Omega_e\left(1-\Omega_e^2/\Omega_0^2\right)}\left(\vec{k}\cdot\vec{E}_{p\perp}\right)^2\right\}n_{\Delta k}$$
$$-i\frac{m_e}{m_i}\frac{e}{m_e}\left\{\begin{array}{l}+\left[(\Omega+i\upsilon_e)^2+\Omega_{pe}^2\right](\Omega_e^2/\Omega_0^2)\left(k_zE_{pz}n_{+k}^*+k_zE_{pz}^*n_{-k}\right)\\ +\Omega_e(\Delta\Omega+i\upsilon_e)\left(k_\perp E_{p\perp}n_{+k}^*+k_\perp E_{p\perp}^*n_{-k}\right)\\ +\frac{\Omega_e\Omega_{pe}^2(\Delta\Omega+i\upsilon_e)}{\Omega_0^2\left(1-\Omega_e^2/\Omega_0^2\right)}\left(k_\perp E_{p\perp}n_{+k}^*-k_\perp E_{p\perp}^*n_{-k}\right)\end{array}\right\} \tag{19}$$

In the following, equations (18) and (19) are employed to analyze the OTSI and PDI excited by X-mode pump wave near the reflection height.

2.2.1. OTSI—Decay to Two Langmuir Waves and a Purely Growing Mode

The pump wave decays to two oppositely propagating Langmuir waves and a purely growing mode in this process; thus, by setting $\omega=\omega_0+i\gamma$ and $\Delta\omega=i\gamma$, equations (18) and (19) combine to

$$\left\{+\Omega_e^2\left[-\gamma(\gamma+\upsilon_i)-k^2c_s^2\right](-k_z^2)-\left\{\begin{array}{l}-(\gamma+\upsilon_e)^2\left[-\gamma(\gamma+\upsilon_i)-k^2c_s^2\right]\\ +\Omega_e\Omega_i\gamma(\gamma+\upsilon_e)\end{array}\right\}(-k_\perp^2)\right\}=$$
$$+\frac{m_e}{m_i}\frac{e^2\Omega_e^2}{m_e^2\Omega_0^2}k^2\left\{+\left(\vec{k}\cdot\vec{E}_{pz}\right)^2+\frac{i\gamma}{\Omega_e\left(1-\Omega_e^2/\Omega_0^2\right)}\left(\vec{k}\cdot\vec{E}_{p\perp}\right)^2\right\}$$
$$+\frac{m_ee^2k^2}{m_i\ m_e^2}\frac{1-\Omega_e^2/\Omega_0^2}{1-\Omega_e^2\cos^2\theta/\Omega_0^2}\frac{2\left(\Omega_0^2-\Omega_L^2+\Sigma\right)\left[(\Omega_0+i\gamma+i\upsilon_e)^2+\Omega_{pe}^2\right](\Omega_e^2/\Omega_0^2)}{\left(\Omega^2-\Omega_L^2+\Sigma\right)^2+\Omega^2\upsilon_e^2}\times$$
$$\left\{\begin{array}{l}+\left(\vec{k}\cdot\vec{E}_{pz}\right)^2\\ +\frac{(i\gamma+i\upsilon_e)}{\sqrt{1+\Omega_e/\Omega_0}}\frac{\Omega_0^2\left[\Omega_0^2-\Omega_L^2+\Sigma+i(\Omega_0+i\gamma)\upsilon_e\Omega_{pe}^2/\left(\Omega_0^2-\Omega_e^2\right)\right]}{\Omega_e\left(\Omega_0^2-\Omega_L^2+\Sigma\right)\left[(\Omega_0+i\gamma+i\upsilon_e)^2+\Omega_{pe}^2\right]}\left(\vec{k}\cdot\vec{E}_{p\perp}\right)^2\end{array}\right\} \tag{20}$$

where $\Omega_L^2=\Omega_{pe}^2+3k^2v_{Te}^2+\Omega_e^2\sin^2\theta$, $\Sigma=\frac{e^2}{m_e^2\Omega_0^2}\frac{1-\Omega_e^2/\Omega_0^2}{1-\Omega_e^2\cos^2\theta/\Omega_0^2}\left[\left(\vec{k}\cdot\vec{E}_{pz}\right)^2+\frac{1}{(1+\Omega_e/\Omega_0)\left(1-\Omega_e^2/\Omega_0^2\right)}\left(\vec{k}\cdot\vec{E}_{p\perp}\right)^2\right]$.

In the heating experiment, when the heating wave and radar beam point along the geomagnetic field, the angle $\theta=0^\circ$. In equation (20), the magnitude of the coefficient of term $\left(\vec{k}\cdot\vec{E}_{p\perp}\right)$ is $\upsilon_e/\Omega_e\sim10^{-5}$; it is assumed that $E_{p\perp}^2/E_{pz}^2<100$, with the corresponding effective radiated power (ERP) indicating that about 1% pump ERP is dispersed in the parallel direction. All $\left(\vec{k}\cdot\vec{E}_{p\perp}\right)$ terms can be approximated to zero and neglected. The threshold is obtained when the growth rate γ approaches 0.

$$E_{zth}^2=\frac{2m_em_i}{e^2}c_s^2\Omega_0^2\left(\Omega_0^2+\Omega_{pe}^2\right)\left[\left(\Omega_0^2-\Omega_1^2\right)+\Omega_0^2\upsilon_{eh}^2\left(\Omega_0^2-\Omega_1^2\right)\right]\frac{1-\Omega_e^2\cos^2\theta/\Omega_0^2}{1-\Omega_e^2/\Omega_0^2} \tag{21}$$

where ω_1 is the frequency of Langmuir wave in the interaction region. The threshold shown in equation (21) varies with the wave number k and the propagation angle θ. For OTSI, there is a preferential height layer to

excite the plasma lines, where $\Omega_0^2-\Omega_1^2\approx\Omega_0\upsilon_e$ and the threshold value achieves the minimum. The minimum threshold can be written as below:

$$E_{zth\min}^2=\frac{4m_em_i}{e^2}c_s^2\Omega_0^3\upsilon_e\left(\Omega_0^2+\Omega_{pe}^2\right)\frac{1-\Omega_e^2\cos^2\theta/\Omega_0^2}{1-\Omega_e^2/\Omega_0^2} \tag{22}$$

2.2.2. PDI—Decay to a Langmuir Wave and an Ion Acoustic Wave

The pump wave decays to a Langmuir wave and an ion acoustic wave in this process. With the similar deduction process for the OTSI, setting $\omega=\omega_r+i\gamma$ and $\Delta\omega=\Delta\omega_r+i\gamma$, then equations (18) and (19) can be combined to give

$$\begin{aligned}
&\left\{\begin{array}{l}-\left[-(\Delta\Omega_r-i\gamma)(\Delta\Omega_r-i\gamma-i\upsilon_{is})+k^2c_s^2\right](-k_z^2)\\ +\dfrac{(\Delta\Omega_r-i\gamma-i\upsilon_e)^2\left[-(\Delta\Omega_r-i\gamma)(\Delta\Omega_r-i\gamma-i\upsilon_i)+k^2c_s^2\right]}{\Omega_e^2}(-k_\perp^2)\\ +\dfrac{\Omega_e\Omega_i(\Delta\Omega_r-i\gamma)(\Delta\Omega_r-i\gamma-i\upsilon_e)}{\Omega_e^2}(-k_\perp^2)\end{array}\right\}\times\\
&\left\{\begin{array}{l}(\Omega_r+i\gamma)^2-\Omega_L^2+i(\Omega_r+i\gamma)\upsilon_e\\ +\dfrac{e^2}{m_e^2\Omega_r^2}\dfrac{1-\Omega_e^2/\Omega^2}{(1-\Omega_e^2\cos^2\theta/\Omega_r^2)}\left[\left(k_z^2E_{pz}^2\right)+\dfrac{1}{(1+\Omega_e/\Omega_0)(1-\Omega_e^2/\Omega_0^2)}\left(k_\perp^2E_{p\perp}^2\right)\right]\end{array}\right\}\\
&-\frac{m_e}{m_im_e^2\Omega_0^2}\left\{+\left(\vec{k}\cdot\vec{E}_{pz}\right)^2+\frac{\Delta\Omega_r-i\gamma}{\Omega_e}1(1-\Omega_e^2/\Omega_0^2)\left(\vec{k}\cdot\vec{E}_{p\perp}\right)^2\right\}\\
&\times\left\{\begin{array}{l}(\Omega_r+i\gamma)^2-\Omega_L^2+i(\Omega_r+i\gamma)\upsilon_e\\ +\dfrac{e^2}{m_e^2\Omega_0^2}\dfrac{1-\Omega_e^2/\Omega_0^2}{(1-\Omega_e^2\cos^2\theta/\Omega_0^2)}\left[\left(\vec{k}\cdot\vec{E}_{pz}\right)^2+\dfrac{1}{(1+\Omega_e/\Omega_r)(1-\Omega_e^2/\Omega_r^2)}\left(\vec{k}\cdot\vec{E}_{p\perp}\right)^2\right]\end{array}\right\}\\
&=\frac{m_e}{m_im_e^2}(1-\Omega_e^2/\Omega_0^2)\left(1+\Omega_{pe}^2/\Omega_0^2\right)(k^2)(1-\Omega_e^2\cos^2\theta/\Omega_0^2)\\
&\times\left\{+\left(\vec{k}\cdot\vec{E}_{pz}\right)^2+\frac{\Delta\Omega_r}{\Omega_e}1(1-\Omega_e^2/\Omega_0^2)1(1+\Omega_e/\Omega_0)\frac{\left[-(\Omega_r+i\gamma+i\upsilon_e)^2+\Omega_e^2-\Omega_{pe}^2\right]}{\left[-(\Omega_r+i\gamma+i\upsilon_e)^2-\Omega_{pe}^2\right]}\left(\vec{k}\cdot\vec{E}_{p\perp}\right)^2\right\}
\end{aligned}\tag{23}$$

In equation (23), the magnitude of the coefficient of term $\left(\vec{k}\cdot\vec{E}_{p\perp}\right)^2$ is $\Delta\omega_r/\Omega_e\sim10^{-3}$. The term $\left(\vec{k}\cdot\vec{E}_{p\perp}\right)^2$ can be neglected when $\theta\approx0^\circ$. Taking $\gamma=0$, the threshold is obtained

$$E_{zth}^2=\frac{4m_im_e}{e^2k^2\cos^2\theta}\Omega_0^3\Delta\Omega\upsilon_e\upsilon_i\left(\Omega_0^2+\Omega_{pe}^2\right)\left[1+\frac{\left(\Omega_0^2-\Omega_1^2\right)^2}{\Omega_0^2\upsilon_e^2}\right]\frac{(1-\Omega_e^2\cos^2\theta/\Omega_0^2)}{(1-\Omega_e^2/\Omega_0^2)} \tag{24}$$

where $\Delta\Omega_r^2=k^2c_s^2-\Delta\Omega\upsilon_i\left(\Omega_1^2-\Omega_0^2\right)/\Omega_0\upsilon_e$, ω_1 is the frequency of Langmuir wave in the interaction region. Similar to the previous case, the threshold is a function of the wave number and the propagation angle. For PDI, the threshold value achieves the minimum and there is a preferential height layer to excite the plasma lines, where $\Omega_0^2-\Omega_1^2=0$ and $\Delta\omega_r=kc_s$, and then the minimum threshold can be obtained as

$$E_{zth\min}^2=\frac{4m_im_e}{e^2k\cos^2\theta}\Omega_0^3c_s\upsilon_e\upsilon_i\left(\Omega_0^2+\Omega_{pe}^2\right)\frac{(1-\Omega_e^2\cos^2\theta/\Omega_0^2)}{(1-\Omega_e^2/\Omega_0^2)} \tag{25}$$

Equations (22) and (25) provide a threshold of the excitation of the parametric instability by extraordinary polarized EM wave and require parallel electric field component of the pump wave E_{pz}. In general, it is assumed that E_{pz} equals to zero in the X-mode heater field due to the small magnitude of E_{pz} compared to $E_{p\perp}$ near the reflection height. However, the parallel component of heater wavefield still exists in the heating experiment, and its small value may be sufficient enough to excite the parametric instability. This small parallel component can arise as a result of the pump wave becoming dispersed as it propagates due to ionospheric inhomogeneity.

3. Comparison With Experimental Observations

In this section, threshold calculations have been performed for different experiments conducted at Tromsø, Norway. The relevant ionospheric parameters are provided by EISCAT website (http://www.eiscat.se/madrigal).

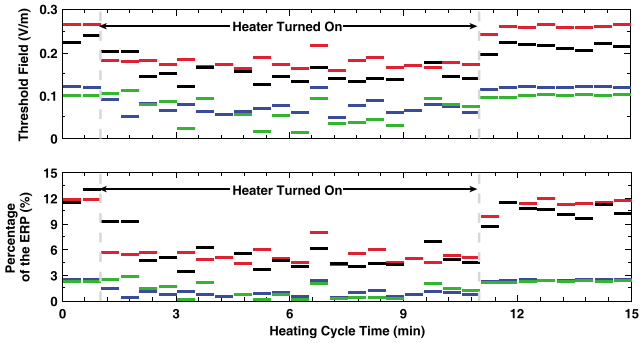

Figure 1. (top) The parametric threshold and (bottom) the percentage between the equivalent ERP of the threshold and the total ERP transmitted from the heater for the experiment on 22 October 2013 (blue), OTSI threshold for the experiment on 22 October 2013 (red), PDI threshold for the experiment on 19 October 2012 (green), and OTSI threshold for the experiment on 19 October 2012 (black); the grey line represents the time when heater is turned off.

The experimental data are processed by the Grand Unified Incoherent Scatter Design and Analysis Package [*Lehtinen and Huuskonen*, 1996]. The neutral densities and collision frequencies are obtained from NRLMSISE-00 [*Picone et al*., 2002], and the geomagnetic field strength is obtained from the International Geomagnetic Reference Field 11 [*Finlay et al*., 2010]. Equations (22) and (25) are employed to calculate the threshold.

Blagoveshchenskaya et al. [2014] reported three X-mode heating experiments ran by the EISCAT heating facility at Tromsø, Norway. The experiments on 19 October 2012 and 22 October 2013 have been operated between 16:00 and 18:00 UT with 10 min on and 5 min off cycles. For the experiment conducted on 19 October 2012, the effective radiated power is 458 MW and the heater frequency is 6.2 MHz, while for the experiment carried out on 22 October 2013, the heater is operated at 7.1 MHz with an ERP of 548 MW. The ERP values listed here take account of the *D* region absorption [*Senior et al*., 2010]. Both the heating wave and the UHF radar beam pointed along the geomagnetic field in these two experiments. As shown in Figures 3 and 5 in *Blagoveshchenskaya et al*. [2014], the HFPLs are observed during the whole heater-on period, associated with electron density and temperature enhancement, which is different from the typical O-mode heating experimental observations when HFPLs are observed only in the first few seconds. The electron density and temperature enhancements depend on the ratio of pump wave frequency to the critical frequency of O-mode HF wave in F_2 layer [*Blagoveshchenskaya et al*., 2015]. The EISCAT heating facility cannot clearly separate the O-mode and X-mode waves. In other words, a possible leakage of O-mode wave can excite PDI and OTSI under X-mode pumping in the overdense ionosphere, i.e., $f_0 < f_o F_2$. Thus, it is very important to clarify whether the HFPLs were excited by X-mode pumping or the leakage of the O-mode wave. The experiment with an alternating O/X-mode heating wave was conducted on 19 October 2012 from 17:01 UT to 17:30 UT. As seen in Figure 4 of *Blagoveshchenskaya et al*. [2014], the interaction height for O-mode was around 260 km at Figure 4a compared to about 250 km for X-mode at Figure 4b. Therefore, HFILs and HFPLs excited by the O/X-mode pump waves can be clearly identified in terms of their interaction heights. The absence of the HFPLs during O-mode pumping cycle possibly results from the excitation of the thermal parametric instability (TPI) near the upper hybrid resonant height, where $\Omega_0^2 = \Omega_{pe}^2 + \Omega_e^2$, below the reflection height. An ordinary polarized electromagnetic wave with about 100 MW ERP can excite the TPI [*Bryers et al*., 2013], by which upper hybrid waves are excited and the power of pump wave is drained off in the interaction area. The EISCAT UHF radar was pointed along the geomagnetic field and could not measure the upper hybrid (UH) wave since an UH wave propagates in a direction nearly perpendicular to that of the geomagnetic field. For the experiment of 19 October 2012 (from 17:16 to 17:26 UT), HFPLs are observed for the whole X-mode pumping cycle without the presence of the downshifted maximum component in the SEE spectrum, which is an effective method to detect the UH wave excited in the heating experiment [*Stubbe et al*., 1984]. Observation of HFPLs indicates that the parametric instability is continuously excited near the X-mode pumping reflection altitude. Under X-mode heating wave, the leakage of the O-mode wave is estimated as 2–3% of full ERP; i.e., ERP of the small fraction of O-mode wave is about ~10–15 MW, much less than the requirement of TPI threshold reported by *Bryers et al*. [2013]. Thus, it can be concluded that TPI is not excited by the small fraction of O-mode wave and does not affect the enhanced HFPLs and HFILs under the X-mode heating wave.

Figure 1 indicates the parametric instability threshold and the value of the equivalent ERP for the experiments on 19 October 2012 and 22 October 2013. As seen in Figure 1, the PDI threshold is lower than the threshold required for OTSI. Also, it is evident that the threshold in the heating on cycle is lower compared to the off cycle. During the heater on cycle, the enhancement of electron density and temperature were

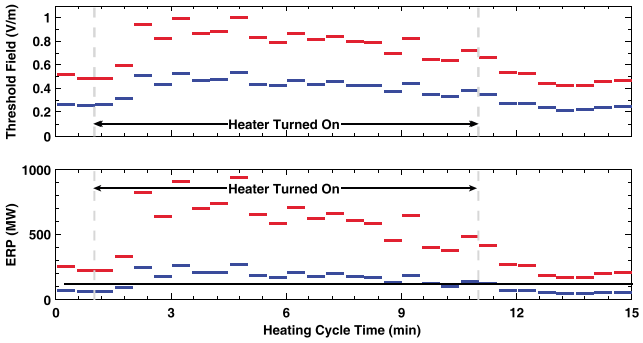

Figure 2. (top) The threshold of the parametric instability blue line is for the PDI and red line for OTSI on the experiment of 8 March 2010; the grey line marks off period. (bottom) The equivalent ERP of the threshold; the black dashed line indicates the 123 MW ERP, which was utilized in this experiment.

observed by UHF radar, which contributes to the decrease of the threshold value. Our calculation indicates that in order to excite the parametric decay instability, 3% of ERP needs to be distributed along the magnetic field; for the excitation of OTSI, the parallel component of ERP needs to be higher (on the order of 12%). This difference in the required parallel component of ERP can explain why the zero-frequency offset enhanced ion line, which is a signature for the excitation of the OTSI that was only observed in the ion line spectra for the experiment conducted on 19 October 2012 (Figure 4 by *Blagoveshchenskaya et al.* [2014]), but this signature was not present in the experiment conducted on 22 October 2013. This power distribution is attributed to the inhomogeneous ionosphere along the path of pump wave.

Another experiment was conducted under X-mode pump wave from 16:00 UT to 17:00 UT on 8 March 2010 with 10 min on and 5 min off cycle [*Blagoveshchenskaya et al.*, 2013]. The ERP of heating wave was 123 MW with the frequency of 5.423 MHz. Both the heating wave and UHF radar beam pointed along the geomagnetic field. In the experiment, HFPLs were not observed. Figure 2 indicates the threshold and equivalent ERP for this experiment. The black dashed line in the bottom plot marks the ERP radiated from the heater facility. The thresholds of PDI and OTSI in the experiment are higher than the experiment performed on 19 October 2012 and 22 October 2013 due to the higher effective collision frequency as illustrated in the bottom plot of Figure 3. The equivalent ERP of the threshold requires at least 50% of the total ERP radiated from the ground. Therefore, our calculation suggests that the parametric instability cannot be excited in this case, as confirmed by the experimental observation.

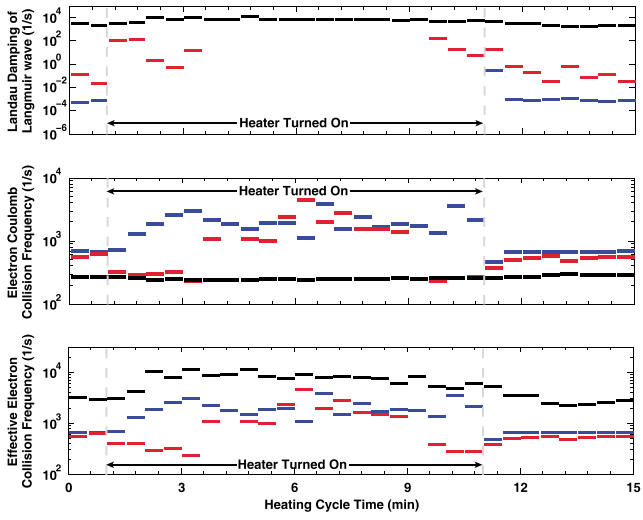

Figure 3. (top) The Landau damping of Langmuir wave, (middle) the electron Coulomb collision frequency, and (bottom) the effective electron collision frequency for the experiment on 22 October 2013 (blue), on 19 October 2012 (red), and on 8 March 2010 (black); the lack of the data during heater on cycle for blue and red lines is because the magnitude of the Landau damping rate is far less than 10^{-6} 1/s.

Figure 3 presents the Landau damping for the Langmuir wave parametrically excited in the experiment. The blue, red, and black lines represent the experiment on 22 October 2013, 19 October 2012, and 8 March 2010, respectively. During the heater on cycle, the Landau damping value for the experiment on 22 October 2013 and 19 October 2012 does not display in the top plot of Figure 3, due to the magnitude far less than 10^{-6} 1/s. The threshold of the parametric instability goes up with an increase in the effective collision frequency. As seen in Figure 3, the Landau damping rate significantly increases the effective collision frequencies for the experiment of 8 March 2010. This can explain the higher threshold on 8 March 2010 compared to the other two experiments carried out on 22 October 2013 and 19 October 2012 and the reason for not observing HFPLs for the experiment

conducted on 8 March 2010. If the Landau damping was neglected in the threshold calculation on 8 March 2010, the thresholds of PDI and OTSI decrease from 0.26 V/m and 0.50 V/m to about 0.07 V/m and 0.15 V/m, respectively. According to the simulation of electric field of pump wave in section 4, PDI could be excited. Since the experimental observation had confirmed that parametric instability was not excited, it testifies to the importance of inclusion of Landau damping in the estimation of the excitation threshold.

4. Simulation

A perfect X-mode polarized EM wave has no component of electric field directed parallel to the geomagnetic field direction. This suggests that it should be impossible for such a wave to excite longitudinal plasma waves, as the parametric decay instability or the oscillating two-stream instability requires a nonzero fraction of the pump wave *E* field to be along the magnetic field near the reflection height. However, because the ionosphere is an inhomogeneous and dispersive medium, it is possible that during propagation, the wave may develop a small parallel field component of sufficient magnitude to exceed the instability threshold. To test this, the full-wave graphical processing unit-accelerated finite difference time domain simulation code described in *Cannon and Honary* [2015] was used to model the propagation of an X-mode polarized EM wave for the experimental conditions described in section 3 above. The code simulates the interaction of the wave with the background plasma in a fully time-explicit manner, allowing the effect of plasma inhomogeneity and anisotropy on wave propagation to be determined. The simulation domain was set up as a 2-D box aligned with the geomagnetic field and terminated on all sides by a perfectly matched absorbing layer. The domain dimensions were set as 30.9 km parallel to the field and 15.5 km perpendicular to the field. A continuous pump wave source with X-mode polarization (*E* field perpendicular to the geomagnetic field) was injected from the lower edge of the domain. Pump beam parameters were set to replicate the experiments described in section 3. A linear electron density gradient in the vertical direction was used as a background profile, with a vertical scale size of 60 km. For each simulation, the density profile was set such that the X-mode reflection height would occur around 28 km above the bottom edge of the simulation domain.

Figure 4 shows the E_{pz} amplitude developed in the simulation for each set of experimental conditions, averaged over 2×10^5 time steps (~2.67 ms). The traces are measured along the pump beam direction and show how the amplitude varies with distance from the lower edge of the simulation domain. In all cases it can be seen that there is a nonzero E_{pz} component, due to the dispersive or refractive effects of the inhomogeneous plasma medium on the propagation of the wave. As the pump wave approaches the X-mode reflection height, corresponding to $\Omega_{pe}^2 = \Omega_0(\Omega_0 - \Omega_e)$, the wave group velocity decreases and a standing wave develops. This leads to a swelling of the amplitude in all components including the parallel field, which can be seen to increase in amplitude with increasing altitude. The parallel field component manages to exceed the amplitude threshold equivalent to ~3% EPR (indicated in the figure by a dashed line) required for the PDI to proceed in the simulations representing the 22 October 2013 and 19 October 2012 experiments. This only occurs for a narrow range of altitudes below the reflection height, where the field has been amplified by the swelling effect of the standing wave. For the case of the simulation representing the 8 March 2010 experiment, the parallel filed amplitude is lower and the required threshold amplitude is not achieved. This agrees well with the experimental observations which report the HFPL signature indicative of PDI on 19 October 2012 and 22 October 2013 but not on 8 March 2010 and supports the analysis of section 3. The simulation results demonstrate that, under certain conditions, the effect of the inhomogeneous plasma background is capable of redirecting a sufficiently large fraction of the X-mode pump energy along the parallel direction for the PDI to be excited.

To excite the OTSI, a parallel *E* field amplitude corresponding to ~12% EPR would be required for the 19 October 2012 and 22 October 2013 experiments. The simulation results show that this is unlikely to be achieved due to the action of the background plasma density gradient alone. To realize E_{pz} fields of this magnitude, more complicated inhomogeneities such as field-aligned density structures must be included in the background density profile. When field-aligned density depletions of maximum amplitude 5% of the background plasma were included in the simulation, this was found to significantly modify the propagation of the X-mode pump wave, with large parallel *E* fields developing within the irregularities. Figure 5 shows the maximum E_{pz} amplitudes recorded in the simulation for a range of irregularity perpendicular scale sizes, for each set of pump wave conditions discussed above. For the cases of the 19 October 2012 and 22 October

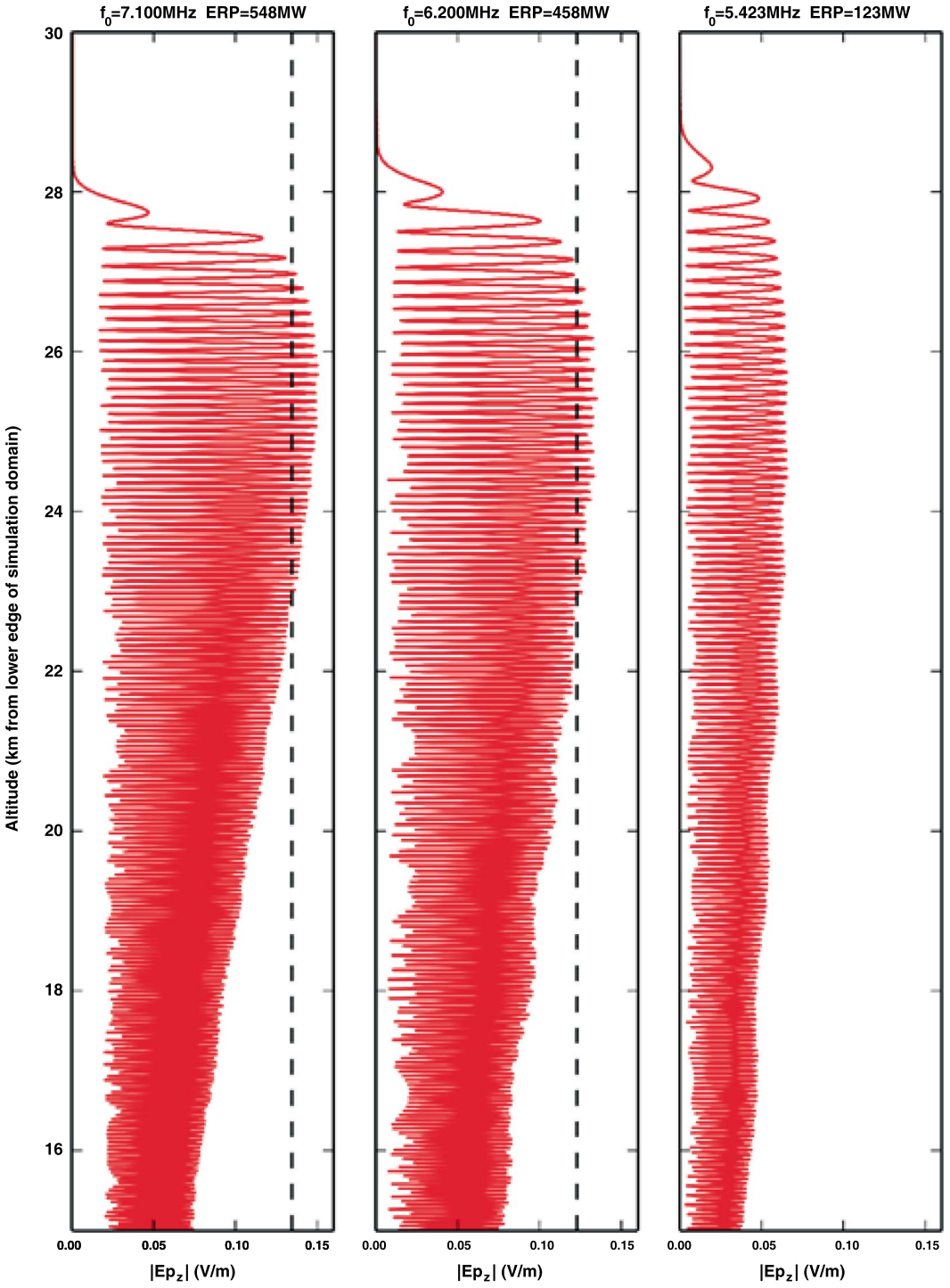

Figure 4. The simulated E_{pz} amplitude around the X-mode reflection height for each set of experimental conditions averaged over 2×10^5 time steps (~2.67 ms). The field amplitude corresponding to 3% of the pump wave ERP is indicated by a dashed line for the cases of the 19 October 2012 and the 22 October 2013 experiments. For the remaining experiment, the PDI threshold corresponded to ~50% of EPR and therefore was much higher than the maximum simulated *E* field amplitude shown here.

2013 experiments, the maximum simulated E_{pz} for most irregularity scale sizes is well in excess of the amplitude threshold equivalent to ~12% EPR (~0.25 V/m) required for the OTSI, particularly for depletions with perpendicular scale size ~1 km. Medium-scale irregularities of this scale have previously been observed to form during X-mode heating [see, for example, *Kosch et al.*, 2007]. This enhancement of the pump electric field

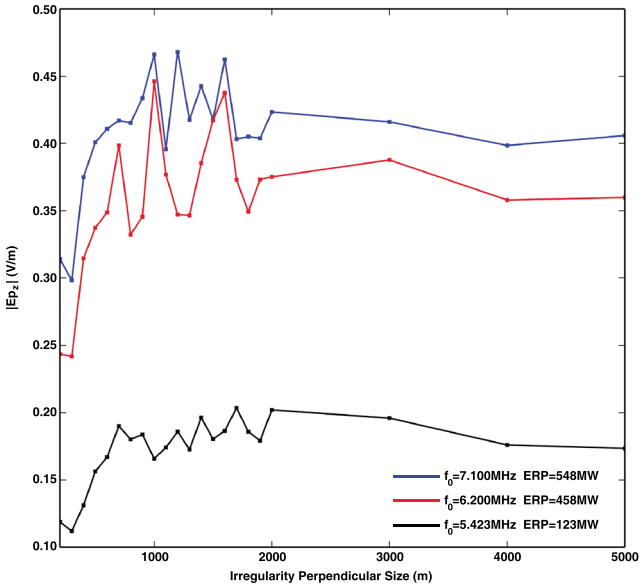

Figure 5. The variation of maximum simulated E_{pz} amplitudes with irregularity perpendicular scale size when field-aligned density depletions with amplitude 5% of background density were included in the simulation. Results are shown for the pump wave conditions of 22 October 2013 (blue), 19 October 2012 (red), and 8 March 2010 (black). For the cases of the 19 October 2012 and 22 October 2013 experiments, the maximum simulated E_{pz} for most irregularity scale sizes is well in excess of the ~12% EPR (~0.25 V/m) threshold required for the OTSI.

through interaction with density irregularities offers a mechanism by which sufficient pump energy could be directed along the magnetic field direction to exceed the instability threshold.

5. Discussion and Summary

The theory of the parametric instability excited by X-mode pump wave is investigated in this paper, which lead to the excitation of Langmuir wave in the ionospheric heating experiments. Previous studies suggest that since the plasma frequency near the X-mode pump reflection height is less than the heater wave frequency, PDI excitation by X-mode pump wave is prohibited. However, when assuming the possibility of parallel component of heater EM wavefield and considering the full dispersion relation of the Langmuir wave [*Baumjohann and Treumann*, 1996], $\Omega^2_{\text{Langmuir}}(k,\theta) = \Omega_p^2 + \Omega_{pe}^2 \int_0^\infty 2\pi v_\perp dv_\perp \int_{-\infty}^{\infty} \frac{k_z v_z^2 \partial f/\partial v_z}{\Omega - k_z v_z} dv_z$, where ω_p is the plasma frequency and f is the electron distribution function, instead of the simple dispersion relation of Langmuir wave, i.e., $\Omega^2_{\text{Langmuir}}(k,\theta) = \Omega_{pe}^2 + 3k^2 v_{te}^2$. It has been illustrated in this paper that the X-mode pump wave has the ability to excite PDI. As demonstrated in Figures 3 and 5 of *Blagoveshchenskaya et al*. [2014], the frequencies of the excited Langmuir waves are close to the pump wave frequency, associated with ion acoustic wave with around 10 kHz, hence satisfying the required frequency matching condition for the excitation of PDI.

It is impossible for the perfect X-mode pump wave to produce a longitudinal electrostatic plasma wave because it only contains perpendicular field component. However, the ionosphere is an inhomogeneous medium. When the X-mode pump wave propagates through the ionosphere, the dispersive effect of the inhomogeneous plasma redirects a small component of the pump wavefield in a direction parallel to the geomagnetic field, which is sufficient to exceed the instability threshold. The simulation results shown in section 4 provide evidence to support this point. Further simulations show that the presence of medium-scale (~1 km) field-aligned density irregularities around the X-mode reflection altitude significantly enhance the parallel component of the pump electric field within the irregularities. This provides a mechanism by which the high threshold for the OTSI could be exceeded by an X-mode wave. The HFPLs observed in the X-mode experiments suggested that the Langmuir wave can be excited by the parametric instability which is weakly damped in the interaction region, due to small Landau damping. The expression of the Landau damping indicates that the Landau damping rate exponentially decays with the heater wave frequency in the interaction region. The Landau damping rate decreases with an increase of the Langmuir wave frequency. Therefore, the Langmuir wave excited by the parametric instability can propagate and be observed by EISCAT UHF radar. The X-mode heating experiments on 22 October 2013 and 19 October 2012 reported the electron density and temperature enhancements. According to the calculation presented in this paper the Landau damping rate for the heater on cycle decreased to ~0. Whereas for the experiment of 8 March 2010, the Landau damping rate maintains a high value, hence restraining the propagation of the Langmuir wave. The derived PDI threshold expression indicates that its value depends on the electron and ion effective collision frequencies, and therefore, it is easier to exceed the threshold of the instability for a higher pump wave frequency, hence explaining the frequency dependence observed in experiments conducted at Tromsø, Norway.

In this paper, the process of parametric instability excited by X-mode pump wave is discussed. The theory provides explanation for the experimental observation of HFPLs and HFILs in the X-mode heating experiments when the heating wave frequency (f_0) is less than critical frequency of F_2 layer (f_oF_2), as reported by *Blagoveshchenskaya et al*. [2014, 2015]. However, *Blagoveshchenskaya et al*. [2014, 2015] demonstrate that enhanced HFILs are observed 12–30 km higher than X-mode reflection height under $f_oF_2 < f_0 < f_xF_2$. In such case, the leakage O-mode EM wave is not expected to reflect and excite parametric instability. The theory presented in this paper cannot explain the production of HFILs at higher altitude under $f_oF_2 < f_0 < f_xF_2$, and the mechanism for this phenomenon requires further investigation. A possible mechanism may be due to mode conversion processes, for example, see *Eliasson* [2013], who reported that O-mode waves can be converted to Z-mode waves propagating to the topside of the ionosphere and converted back to O-mode waves exciting Langmuir wave on the topside.

Acknowledgments
EISCAT is an international scientific association supported by research organizations in China (CRIRP), Finland (SA), Japan (NIPR and STEL), Norway (NFR), Sweden (VR), and UK (NERC). This work was supported by the National Natural Science Foundation of China (NSFC grants 41204111 and 41574146). W.X. appreciated the support by China Scholar Council (201406270061). C.Z. appreciates the support by Wuhan University "351 Talents Project." The data used in this paper are available through the EISCAT Madrigal database (http://www.eiscat.se/madrigal/).

References

Baumjohann, W., and R. A. Treumann (1996), *Basic Space Plasma Physics*, Imperial College Press, London.
Bernhardt, P. A., C. A. Tepley, and L. M. Duncan (1989), Airglow enhancements associated with plasma cavities formed during ionospheric heating experiments, *J. Geophys. Res.*, *94*, 9071–9092, doi:10.1029/JA094iA07p09071.
Blagoveshchenskaya, N. F., T. D. Borisova, T. Yeoman, M. T. Rietveld, I. M. Ivanova, and L. J. Baddeley (2011), Artificial field-aligned irregularities in the high-latitude *F* region of the ionosphere induced by an X-mode HF heater wave, *Geophys. Res. Lett.*, *38*, L08802, doi:10.1029/2011GL046724.
Blagoveshchenskaya, N. F., T. D. Borisova, T. K. Yeoman, M. T. Rietveld, I. Häggström, and I. M. Ivanova (2013), Plasma modifications induced by an X-mode HF heater wave in the high latitude *F* region of the ionosphere, *J. Atmos. Sol. Terr. Phys.*, *105-106*, 231–244.
Blagoveshchenskaya, N. F., T. D. Borisova, M. Kosch, T. Sergienko, U. Brändström, T. K. Yeoman, and I. Häggström (2014), Optical and ionospheric phenomena at EISCAT under continuous X-mode HF pumping, *J. Geophys. Res. Space Physics*, *119*, 10,483–10,498, doi:10.1002/2014JA020658.
Blagoveshchenskaya, N. F., T. D. Borisova, T. K. Yeoman, I. Häggström, and A. S. Kalishin (2015), Modification of the high latitude ionosphere *F* region by X-mode powerful HF radio waves: Experimental results from multi-instrument diagnostics, *J. Atmos. Sol. Terr. Phys.*, *135*, 50–63, doi:10.1016/j.jastp.2015.10.009.
Bryers, C. J., M. J. Kosch, A. Senior, M. T. Rietveld, and T. K. Yeoman (2013), The thresholds of ionospheric plasma instabilities pumped by high-frequency radio waves at EISCAT, *J. Geophys. Res. Space Physics*, *118*, 7472–7481, doi:10.1002/2013JA019429.
Cannon, P., and F. Honary (2015), A finite difference time domain scheme for electromagnetic wave interaction with plasma, *IEEE Trans. Antennas Prop.*, *63*(7), 3042–3054, doi:10.1109/TAP.2015.2423710.
Eliasson, E. (2013), Full-scale simulations of ionospheric Langmuir turbulence, *Mod. Phys. Lett. B*, *27*(8), 1330005, doi:10.1142/S0217984913300056.
Fejer, J. A. (1979), Ionospheric modification and parametric instabilities, *Rev. Geophys.*, *17*(1), 135–153, doi:10.1029/RG017i001p00135.
Fejer, J. A., and E. Leer (1972), Purely growing parametric instability in an inhomogeneous plasma, *J. Geophys. Res.*, *77*(4), 700–708, doi:10.1029/JA077i004p00700.
Fialer, P. A. (1974), Field-aligned scattering from a heated region of the ionosphere—Observations at HF and VHF, *Radio Sci.*, *9*(11), 923–940, doi:10.1029/RS009i011p00923.
Finlay, C. C., et al. (2010), International geomagnetic reference field: The eleventh generation, *Geophys. J. Int.*, *183*(3), 1216–1230, doi:10.1111/j.1365-246X.2010.04804.x.
Frey, A. (1986), The observation of HF-enhanced plasma waves with the EISCAT/UHF-radar in the presence of strong Landau-damping, *Geophys. Res. Lett.*, *13*, 438–441, doi:10.1029/GL013i005p00438.
Frolov, V. L., et al. (2014), Generation of artificial ionospheric irregularities in the midlatitude ionosphere modified by high-power high-frequency X-mode radio waves, *Radiophys. Quantum Electron.*, *57*, 393–416, doi:10.1007/s11141-014-9523-8.
Gurevich, A. V. (1978), *Nonlinear Phenomena in the Ionosphere*, *Ser. Phys. Chem. Space*, vol. 10, Springer, New York.
Kosch, M. J., M. T. Rietveld, A. J. Kavanagh, C. Davis, T. K. Yeoman, F. Honary, and T. Hagfors (2002), High-latitude pump-induced optical emissions for frequencies close to the third electron gyro-harmonic, *Geophys. Res. Lett.*, *29*(23), 2112, doi:10.1029/2002GL015744.
Kosch, M. J., T. Pedersen, M. T. Rietveld, B. Gustavsson, S. M. Grach, and T. Hagfors (2007), Artificial optical emissions in the high latitude thermosphere induced by powerful radio waves: An observational review, *Adv. Space Res.*, *40*, 365–376.
Kuo, S. (1996), The role of nonlinear beating currents on parametric instabilities in magnetoplasmas, *Phys. Plasmas*, *3*, 3957, doi:10.1063/1.871568.
Kuo, S. (2002), Oscillating two-stream instability in ionospheric heating experiments, *Phys. Plasmas*, *9*(4), 1456–1459, doi:10.1063/1.1453471.
Kuo, S. (2015), Ionospheric modifications in high frequency heating experiments, *Phys. Plasmas*, *22*, 012901, doi:10.1063/1.4905519.
Kuo, S. P., B. R. Cheo, and M. C. Lee (1983), The role of parametric decay instabilities in generating ionospheric irregularities, *J. Geophys. Res.*, *88*(A1), 417–423, doi:10.1029/JA088iA01p00417.
Kuo, S., A. Snyder, and M. C. Lee (2014), Experiments and theory on parametric instabilities excited in HF heating experiments at HAARP, *Phys. Plasmas*, *21*, 062902, doi:10.1063/1.4885642.
Lehtinen, M. S., and A. Huuskonen (1996), General incoherent scatter analysis and GUISDAP, *J. Atmos. Sol. Terr. Phys.*, *58*, 435–452.
Leyser, T. B., and A. Y. Wong (2009), Powerful electromagnetic waves for active environmental research in geospace, *Rev. Geophys.*, *47*, RG1001, doi:10.1029/2007RG000235.
Minkoff, J., P. Kugelman, and I. Weissman (1974), Radio frequency scattering from a heated ionospheric volume: 1. VHF/UHF field-aligned and plasma-line backscatter measurements, *Radio Sci.*, *9*(11), 941–955, doi:10.1029/RS009i011p00941.
Muldrew, D. B., and R. L. Showen (1977), Height of the HF-enhanced plasma line at Arecibo, *J. Geophys. Res.*, *82*(29), 4793–4804, doi:10.1029/JA082i029p04793.
Pedersen, T., and H. Carlson (2001), First observations of HF heater-produced airglow at the High Frequency Active Auroral Research Program facility: Thermal excitation and spatial structuring, *Radio Sci.*, *36*, 1013–1026, doi:10.1029/2000RS002399.
Perkins, F. W., C. Oberman, and E. J. Valeo (1974), Parametric instabilities and ionospheric modification, *J. Geophys. Res.*, *79*(10), 1478–1496, doi:10.1029/JA079i010p01478.
Picone, J. M., A. E. Hedin, D. P. Drob, and A. C. Aikin (2002), NRLMSISE-00 empirical model of the atmosphere: Statistical comparisons and scientific issues, *J. Geophys. Res.*, *107*(A12), 1468, doi:10.1029/2002JA009430.

Rietveld, M. T., B. Isham, H. Kohl, C. La Hoz, and T. Hagfors (2000), Measurements of HF-enhanced plasma and ion lines at EISCAT with high-altitude resolution, *J. Geophys. Res.*, *105*(A4), 7429–7439, doi:10.1029/1999JA900476.

Robinson, T. R. (1989), The heating of the high latitude ionosphere by high power radio wave, *Phys. Rep.*, *179*, 79–209.

Senior, A., M. T. Rietveld, M. J. Kosch, and W. Singer (2010), Diagnosing radio plasma heating in the polar summer mesosphere using cross modulation: Theory and observations, *J. Geophys. Res.*, *115*, A09318, doi:10.1029/2010JA015379.

Senior, A., M. T. Rietveld, I. Häggström, and M. J. Kosch (2013), Radio-induced incoherent scatter ion line enhancements with wide altitude extents in the high-latitude ionosphere, *Geophys. Res. Lett.*, *40*, 1669–1674, doi:10.1002/grl.50272.

Stubbe, P., H. Kopka, and B. Thide (1984), Stimulated electromagnetic emission: A new technique to study the parametric decay instability in the ionosphere, *J. Geophys. Res.*, *89*, 7523–7536, doi:10.1029/JA089iA09p07523.

Thome, G. D., and D. W. Blood (1974), First observations of RF backscatter from field-aligned irregularities produced by ionospheric heating, *Radio Sci.*, *9*(11), 917–921, doi:10.1029/RS009i011p00917.

Utlaut, W. F., and R. Cohen (1971), Modifying the ionosphere with intense radio waves, *Science*, *174*(4006), 245–254, doi:10.1126/science.174.4006.245.